Study of Corrosion Characteristics of AlMg3.5 Alloy by Hydrogen-Induced Pressure and Mass Loss Evaluation Under Simulated Cementitious

corrosion and materials degradation

MDPI

Article

Study of Corrosion Characteristics of AlMg3.5 Alloy by Hydrogen-Induced Pressure and Mass Loss Evaluation Under Simulated Cementitious Repository Conditions

Marvin Schobel [1,*], Christian Ekberg [1], Teodora Retegan Vollmer [1], Fredrik Wennerlund [2], Svante Hedström [3] and Anders Puranen [1,4,*]

[1] Nuclear Chemistry, Department of Chemistry and Chemical Engineering, Chalmers University of Technology, 412 96 Gothenburg, Sweden; che@chalmers.se (C.E.); tretegan@chalmers.se (T.R.V.)
[2] Tandläkare Fredrik Wennerlund, 439 55 Åsa, Sweden; fredrik@famwennerlund.com
[3] SKB AB, 169 03 Solna, Sweden; svante.hedstrom@skb.se
[4] AB SVAFO, 612 33 Nyköping, Sweden
* Correspondence: schobel@chalmers.se (M.S.); anders.puranen@svafo.se (A.P.)

Abstract

The decommissioning and dismantling of nuclear research reactors can lead to a large amount of low- and intermediate-level radioactive waste. For repositories, the materials must be kept confined and safety must be ensured for extended time spans. Waste is encapsulated in concrete, which leads to alkaline conditions with pH values of 12 and higher. This can be advantageous for some radionuclides due to their precipitation at high pH. For other materials, such as reactive metals, however, it can be disadvantageous because it might foster their corrosion. The Studsvik R2 research reactor contained an AlMg3.5 alloy with a composition close to that of commercial Al5154 for its core internals and the reactor tank. Aluminum corrosion is known to start rapidly due to the formation of an oxidation layer, which later functions as natural protection for the surface. The corrosion can lead to pressure build-up through the accompanied production of hydrogen gas. This can lead to cracks in the concrete, which can be pathways for radioactive nuclides to migrate and must therefore be prevented. In this study, unirradiated rod-shaped samples were cut from the same material as the original reactor tank manufacture. They were embedded in concrete with elevated water–cement ratios of 0.7 compared to regular commercial concrete (ca. 0.45) to ensure water availability throughout all of the experiments. The sample containers were stored in pressure vessels with attached high-definition pressure gauges to read the hydrogen-induced pressure build-up. A second set of samples were exposed in simplified artificial cement–water to study similarities in corrosion characteristics between concrete and cement–water. Additionally, the samples were exposed to concrete and cement–water in free-standing sample containers for deconstructive examinations. In concrete, the corrosion rates started extremely high, with values of more than 10,000 µm/y, and slowed down to less than 500 µm/y after 2000 h, which resulted in visible channels inside the concrete. In the cement–water, the samples showed similar behavior after early fluctuations, most likely caused by the surface coverage of hydrogen bubbles. These trends were further supported by mass loss evaluations.

Keywords: corrosion; repository; aluminum; hydrogen; cement

Received: 22 April 2025
Revised: 10 June 2025
Accepted: 27 June 2025
Published: 30 June 2025

Citation: Schobel, M.; Ekberg, C.; Retegan Vollmer, T.; Wennerlund, F.; Hedström, S.; Puranen, A. Study of Corrosion Characteristics of AlMg3.5 Alloy by Hydrogen-Induced Pressure and Mass Loss Evaluation Under Simulated Cementitious Repository Conditions. *Corros. Mater. Degrad.* **2025**, *6*, 27. https://doi.org/10.3390/cmd6030027

1. Introduction

Decommissioned nuclear reactors produce low- and intermediate-level radioactive waste, which necessitates proper disposal to ensure environmental and public safety [1,2]. This waste requires repositories with extended lifetimes capable of withstanding both natural degradation and waste-induced alteration processes [2]. Encapsulating decommissioned and other low- and intermediate-level radioactive waste in concrete, as conducted in Swedish repositories, can serve as an effective barrier, as the high pH and low permeability of concrete are known to promote long-term radionuclide retention through sorption and limited solubility [3–5]. However, the initially high pH of more than 13 in concrete porewater, which eventually decreases to below 10 through carbonation over time, can adversely impact the corrosion resistance of reactive metals like aluminum [1,4,6]. Aluminum and its alloys are commonly employed in nuclear research reactors [1]. These materials are susceptible to fast initial corrosion under alkaline environments. Corrosion then gradually slows down, owing to the rapid formation of an oxide layer through surface oxidation by water. This oxide coating impedes, while not eliminating, further corrosion, effectively slowing the generation of aluminum oxides and hydroxides over a timeframe ranging from seconds to weeks, contingent on the material's surface characteristics [1,6]. Solid corrosion products under repository conditions primarily consist of amorphous Al_2O_3 in the initial stage (Equation (1)), followed by the formation of thermodynamically unstable AlOOH (Equation (2)) and $Al(OH)_3$ (Equation (3)) and with the development of the oxide layer, as observed at pH values exceeding 12 [1,6–8]. The dominating species in the aqueous phase, the $[Al(OH)_4]^-$ ion, as described in Equation (4), is believed to be the primary driver for the eventual dissolution of the oxide layer under high-pH conditions [8]. Furthermore, hydrogen gas build-up can induce pressure that may lead to the formation of cracks and channeling in the concrete [1,4,6,9,10]. These cracks can then serve as pathways for the ingress of groundwater and migration of radionuclides, potentially compromising the long-term safety assessment of the repository [1,2].

$$2Al + 3H_2O \rightarrow Al_2O_3 + 3H_2 \quad (1)$$

$$2Al + 4H_2O \rightarrow 2AlOOH + 3H_2 \quad (2)$$

$$2Al + 6H_2O \rightarrow 2Al(OH)_3 + 3H_2 \quad (3)$$

$$2Al + 6H_2O \rightarrow 2Al(OH)_4^- + 3H_2 \quad (4)$$

While limited research has been conducted on aluminum corrosion under repository or simulated repository conditions, the available studies have reported high initial corrosion rates in the range of 10^3 µm/y after two weeks to 20 days [1,6]. However, these rates declined rapidly, attributed to the formation of a protective oxide layer, eventually reaching values around 10^2 µm/y within 26 to 80 days [1,6]. Previous investigations have primarily utilized electrochemical methods (e.g., [7,9]) or mass loss evaluations (e.g., [1,6,11]) to assess aluminum corrosion behavior under alkaline environments. Furthermore, it is well-established that the presence or absence of oxygen does not influence the corrosion of aluminum [12]. The decommissioned Studsvik R2 reactor contained an AlMg3.5 alloy for its core internals and reactor tank, with a similar composition to 5154 aluminum alloy. As the magnesium content is less than 7%, stress corrosion cracking of this material can be excluded from consideration [13]. Nevertheless, the evolution of hydrogen gas, a known by-product of magnesium corrosion, must be taken into account (e.g., [14–18]). Since no data was available on the alkaline corrosion behavior of this specific alloy, an investigation was conducted in this study. For this purpose, rods cut from the original AlMg3.5 alloy batch of the decommissioned R2 reactor were subjected to corrosion testing, simulating cementitious conditions of a Swedish repository for low- and intermediate-

level radioactive waste. Pristine samples encased in concrete with an elevated water content simulate severe initial corrosion conditions. A set of experiments in simplified simulated granitic cement–water was also evaluated. The simulated cement–water solution was deliberately simplified to only contain 10 mM NaCl, which approximates the salt content in granitic groundwater. An excess of solid CaO immersed in a perforated tube creates a saturated $Ca(OH)_2$ solution with a pH of 12.4, simulating simplified weathered cement–water conditions. The experiment was performed at room temperature (ca. 19 °C). Corrosion rates were calculated based on hydrogen-induced pressure measurements and were compared to the mass loss. X-ray imaging was performed with separate samples in concrete and cement–water. This study is a follow-up examination of a previous paper based on the same alloy with a simplified overpressure bottle setup [19].

2. Materials and Methods

Sample preparation. Cylindrical samples, measuring 15 mm in length and 5 mm in diameter, were fabricated by cutting and machining from unirradiated reference samples obtained during the production of the Studsvik R2 reactor tank. The average roughness factors resulting from the machining process are not expected to substantially alter the order of magnitude of the results, particularly considering that the evolution of surface area through the corrosion would likely induce a more significant change in surface area.

Production of concrete. To produce 250 g of concrete, 65.8 g of standard CEM 1 Portland cement (Chalmers Building Materials Lab, Gothenburg, Sweden), 13.2 g of calcium carbonate (Limus 40, Nordkalk, Köping, Sweden), 132 g of standard sand (EN 196-1 standard sand), and 46.1 mL of ultrapure water (Milli-Q, Merck Life Science AB, Solna, Sweden, 18.2 MΩ·cm at 25 °C) were used. Higher water–cement ratios of 0.7 compared to commercial concrete were obtained to guarantee the continuation of the corrosion due to a higher pore water content.

Production of cement–water (CW). The artificial CW was produced in a very simplified manner by dissolving 0.74 g of NaCl as background electrolytes in 200 mL MQ water (10 mM NaCl). The pH was buffered and kept at a constant level of 12.4 by adding 0.43 g of CaO to 1.5 mL microcentrifuge tubes (Eppendorf, Hamburg, Germany) with a perforated lid to create an excess of solid CaO. The constant pH was confirmed by pH paper (VWR chemicals, Radnor, PA, USA). Considering pH and composition, the water reflects old/weathered cement conditions in crystalline bedrock and can therefore display longer-term repository conditions better than fresh concrete.

Pressure measurements. Samples were immersed in 20 mL of concrete in plastic test tubes and stored in 165 mL pressure vessels (Precision Fabrication LLC, Ligonier, IN, USA) (Figure 1). Leak tests were repeatedly performed with a semi-conductor hydrogen detector (Multitec 540, Sewerin, Gütersloh, Germany), with no indication of leakages. The pressure was measured with a pressure gauge designed for hydrogen use (LEO-Record-H2Ei, Keller, Basel, Switzerland). The measured pressure was observed in PressureSuite (Keller, Switzerland). The sample size was selected so that the possible pressure of full corrosion of the samples would not exceed the operating pressure (3447 kPa) of the vessels (design pressure 6895 kPa). The experiment was conducted in duplicates at room temperature (ca. 19 °C).

Figure 1. Pressure vessel setup for hydrogen pressure measurements. Customized steel autoclave with pressure gauge designed for hydrogen use.

Mass loss evaluation. Separate samples in triplicates were immersed in concrete and CW in unpressurized containers at room temperature and were exposed for one to twelve months. Afterwards, destructive measurements were conducted by cracking open the concrete and pickling the samples. Full removal of the concrete and oxide layer was performed by pickling the samples in an ultrasonic bath (Thermo Fisher Scientific, Waltham, MA, USA) for 20 min in 20% nitric acid. Thereafter, the samples were soaked in silicon oil for about 24 h to soften and loosen residues of the oxide layer. The residues were carefully scraped off and the samples were pickled in 20% nitric acid again. This process was repeated until no further mass loss was registered. The samples were cleaned in acetone, dried, and weighed, and the mass loss was determined by weighing. Figure 2 shows a sample after one year of exposure in concrete (left) and after fully removing the concrete and oxide layer (right).

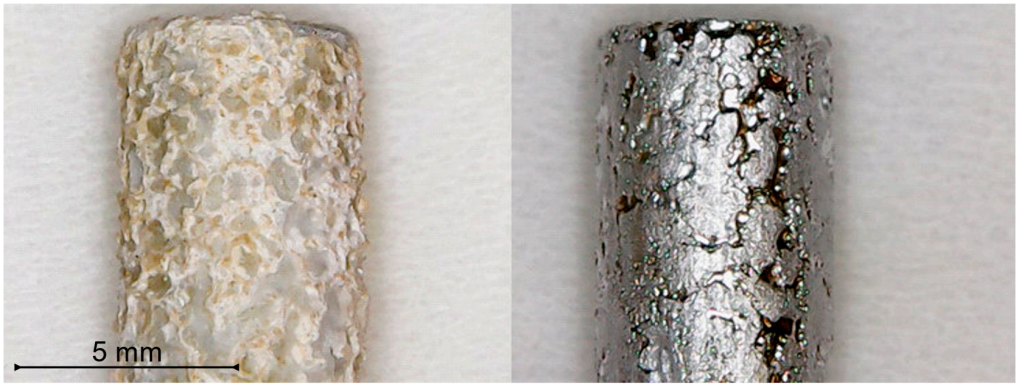

Figure 2. Retrieved R2 alloy sample after one year of exposure embedded in concrete (**left**) and sample after fully removing concrete residues and oxide (**right**).

Calculation of corrosion rates. Equations (1)–(4) were used for the calculation of the corrosion rates. Al_2O_3 was assumed to be an product of the oxide layer formed early on. $Al(OH)_3$ was assumed to be the main solid corrosion product. The pressure increase was recorded and then used to calculate the amount of substance n H_2 and from that, n Al. Considering the molar mass M of Al, it was possible to calculate the mass m of Al. Based on the mass, the corrosion rate could be calculated in $g/m^2/y$. After including the geometric surface area, it was also possible to calculate the corrosion depth and therefore the corrosion rate in µm/y. Corrosion rates were also studied using mass loss. At mass loss evaluation, the rate was calculated and extrapolated to µm/y from the respective corrosion-induced weight loss.

X-ray imaging. X-ray scans were made as an exploratory supporting analysis with an Oralix AC (65 kVp, Gendex Corp., Hatfield, PA, USA). Samples in CW were measured with an exposure time of 0.12 s while the ones in concrete were exposed for 1.6 s. The pictures were exported with the preferred imaging extension tool of the software Dentalmind Digital X-ray II (Dentalmind, Falkenberg, Sweden).

3. Results

3.1. Corrosion Rates

The corrosion rates from the gas pressure measurements in µm/y of the R2 alloy in concrete over a time period of 2000 h are shown in black in Figure 3. Uncertainties were calculated, using duplicates of the samples in identical setups, as standard deviations with Bessel's correction. The corrosion rates start at very high values of more than 10,000 µm/y and then decrease significantly after only a few days. After 2000 h, the rate is below 500 µm/y. The blue points are the corrosion rates of the R2 alloy calculated by mass loss evaluation after six months and one year. The rates were 684 µm/y after one month, 161 µm/y after six months, and 155 µm/y after one year. A power fit with a 95% confidence interval is shown to highlight the compatibility of both methods.

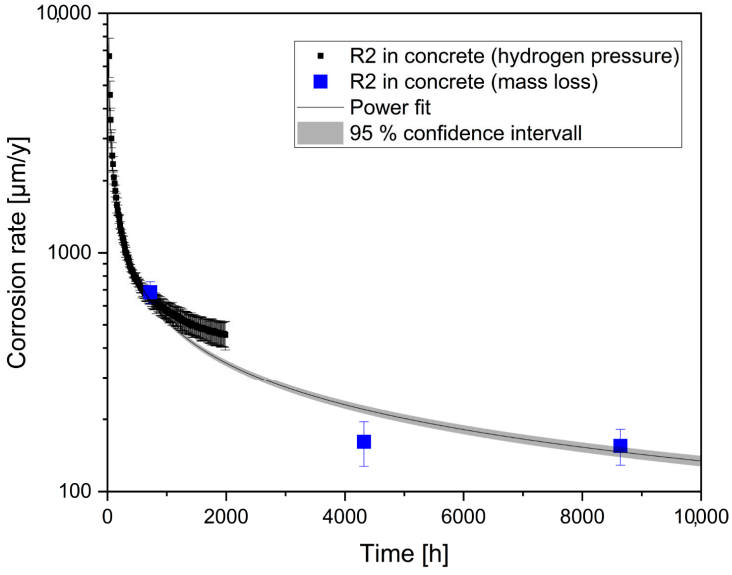

Figure 3. Corrosion rate of R2 alloy in concrete over a time period of 2000 h calculated by H_2-induced pressure (black) in logarithmic scale. Uncertainties calculated from sample duplicates as standard deviations with Bessel's correction. Corrosion rate of R2 alloy in concrete calculated by mass loss evaluation (blue). Uncertainties calculated from sample triplicates. Power fit with 95% confidence interval to highlight compatibility of methods.

The corrosion rates of the R2 alloy in CW over a period of 1700 h are shown in black in Figure 4. Uncertainties were calculated using duplicates of the samples as a standard

deviations with Bessel's correction. A closer view of the early rates can be seen in the cutout. The corrosion rates have high uncertainties initially. After approximately 100 h, they start to rise up to 800 µm/y, while the uncertainties decrease. Afterwards, a decrease is noticeable, to rates of approximately 100 µm/y. The blue points represent the corrosion rate of the R2 alloy in CW calculated from mass loss evaluation after six months and after one year. The corrosion rates were 55 µm/y after six months and 3 µm/y after one year.

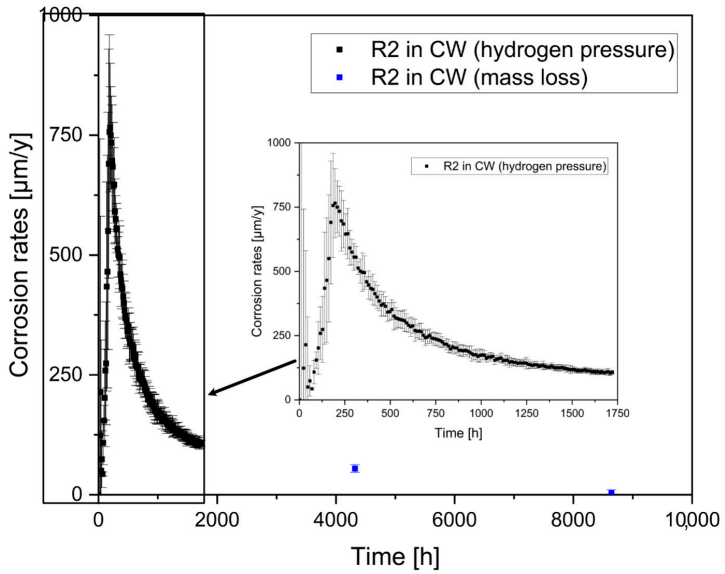

Figure 4. Corrosion rate of R2 alloy in CW over a time period of 1700 h calculated by H_2-induced pressure (black). Uncertainties calculated from sample duplicates as standard deviations with Bessel's correction. Cutout shows the rates detailed. Corrosion rate of R2 alloy in CW calculated by mass loss evaluation (blue). Uncertainties calculated from sample triplicates.

The corrosion rates in CW were plotted against the corrosion rates in concrete in Figure 5. A time span of approximately 275 h between 225 and 500 h of exposure time was chosen. The uncertainties were calculated as standard deviations with Bessel's correction from the sample duplicates. A linear trend with $R^2 = 0.98$ was fitted to highlight the linear dependency of the corrosion of the R2 alloy in both media.

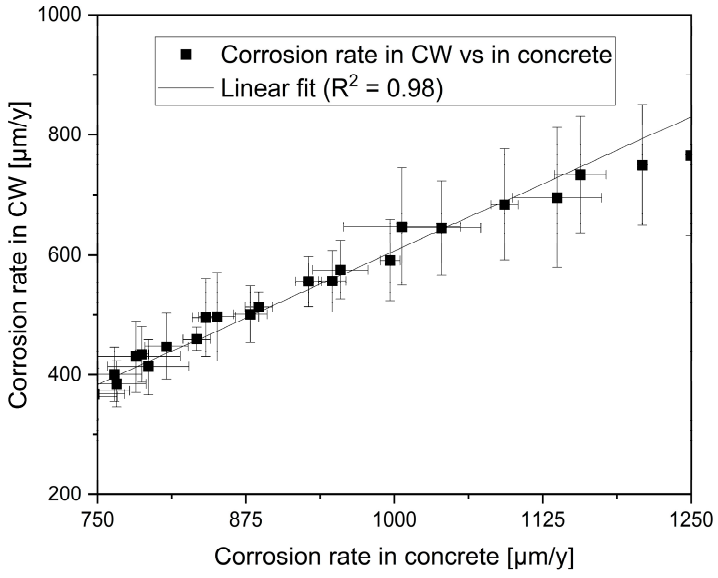

Figure 5. Corrosion rate in CW against corrosion rate in concrete over a time span of ca. 275 h between 225 and 500 h of exposure to highlight linear dependency. Uncertainties calculated from sample duplicates as standard deviations with Bessel's correction.

3.2. X-Ray Imaging

An X-ray scan of an uncorroded sample of the R2 alloy showed the visible outer edges of the sample, as seen in Figure 6. The second sample was corroded for nine months in artificial CW. The edges do not seem to be as clearly visible anymore. The third sample was exposed for 12 months in concrete. The scan was conducted in situ through the concrete; therefore, the samples could be exposed further during and after the measurement. The outline was clearly noticeable, and the oxide layer could be seen to have a darker color on the X-ray scans. The exact orientation of the sample in concrete is not determinable; however, an approximate thickness of the oxide layer could be assumed. The evolution of hydrogen bubbles on the sample surface could also contribute to the darker color.

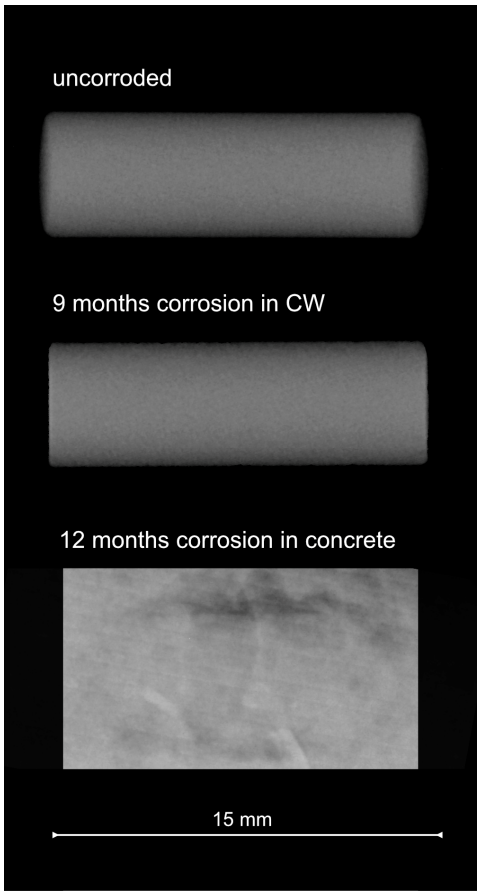

Figure 6. X-ray scans of uncorroded R2 alloy sample, sample that was corroded for 9 months in CW, and embedded sample that was corroded for 12 months in concrete. Exact orientation of sample in concrete cannot be determined.

4. Discussion

4.1. Corrosion Rates by H_2-Induced Pressure Build-Up

The corrosion rates of the alloy in concrete up to 2000 h are shown in Figure 3. High corrosion rates in the beginning come with higher uncertainties due to the immediate start of the corrosion [1,6,7,19]. Small time differences in starting the experiment in the setup can quickly lead to high uncertainties, which diminishes as the experiment proceeds. The high corrosion rates of more than 10,000 µm/y are assumed to be caused by the early formation of an oxide layer on the sample surface, mainly composed of amorphous Al_2O_3 in acute corrosion and crystalline $Al(OH)_3$ in chronic corrosion [1,6–8,19]. The rates decreased strongly only after a few hours because the oxidation layer functioned as protection and therefore as a natural prevention of further rapid corrosion rates [1,6–8,19]. Corrosion

slowed down constantly afterwards. Other factors contributing to the decrease in the corrosion rate, such as the dehydration of concrete, precipitation of $Ca(OH)_2$, or changes in pH due to corrosion processes, were assumed to be negligible due to the given W/C ratio in the experiments and the limited amount of exposure time [20,21].

The corrosion rates of the R2 alloy in CW calculated using the build-up of hydrogen pressure are shown in Figure 4. The cutout shows a closer view after 1700 h of exposure time. Strong uncertainties were detected in the initial stage of the experiments. This was most likely caused due to small differences between the replicates in the preparation times of the experiments and also due to the initial formation of hydrogen bubbles on the surface of the samples [19]. These could, depending on the relative coverage of the surface, prevent the alloy from rapid corrosion. After approximately 100 h, the corrosion rate increased rapidly up to rates of 800 µm/y, which might be caused by the release of the hydrogen bubbles and therefore the disappearance of the potentially protective gas layer. Acute corrosion and the formation of the oxide layer lead to a strong increase in the corrosion rate [1,6–8,19]. Another factor with a smaller impact on the delayed increase in the corrosion rates could be the diffusion of hydrogen in the cement–water solution [22]. After only a short period of time, the corrosion rates decreased again due to the protection provided by the oxide layer of the sample surface [1,6–8,19]. The overall lower corrosion rates in the simulated old cement–water compared to the concrete are consistent with the slightly higher pH in the concrete and our previous report on the R2 alloy [19]. This is also supported by a linear dependency between corrosion in CW and concrete, with $R^2 = 0.98$ after 225 to 500 h, as seen in Figure 5. It can be assumed that the CW conditions predict the corrosion rate in concrete in the longer term. A study showed significantly higher corrosion rates at the beginning of their experiment [19]. This could not be seen in the present study and can be explained by the longer preparation time after exposure in the setup and, therefore, the decrease in the initial corrosion rates. Fluctuations due to the hydrogen bubbles were also not seen in the previous study [19]. This can be explained by the higher sensitivity of the setup used in this study and the corrosion rates being the average of specific time spans in the previous study, which most likely canceled out the effect observed.

4.2. Corrosion Rates by Mass Loss Evaluation

The corrosion rates of the R2 alloy calculated by mass loss evaluation are shown in Figures 3 and 4 after the samples were exposed for six months and one year in concrete and CW. The higher corrosion rates after this period of time for the samples in concrete compared to those in CW were consistent with the results of the H_2 pressure-induced calculations and with the findings of the previous study [19]. However, the corrosion rates in both media, concrete and CW, were relatively low and the differences between them were considered to be negligible in the long term (several years), which is consistent with the conditions of the artificial cement–water replicating those of weathered cement in crystalline bedrock, and represents longer-term exposure than that with the fresh cement [3,23–25]. To compare the corrosion rates in concrete calculated by H_2-induced pressure and by mass loss evaluation, a power fit was used. After one month in concrete, the extrapolated corrosion rate was 650 µm/y, while the one calculated by mass loss was 684 µm/y. After six months, the extrapolated rate was 220 µm/y, which is slightly higher than the rate calculated by mass loss. However, after 12 months, the extrapolated rate was 147 µm/y, which is in the uncertainty range of the mass loss evaluated rate. The difference after six months could be considered to be caused by the long-term extrapolation. Overall, the lower corrosion rates in CW compared to concrete due to the additional protection from hydrogen bubbles and the lower pH were also seen in the mass loss evaluation. The trends were consistent with the previous study on the same material with the simplified overpressure bottle setup [19].

In conclusion, the corrosion rates of the R2 alloy seemed to be slower than those in previous studies on pure aluminum metal [1]. Larger differences were seen in CW, which could be caused by different compositions of the solution [1]. The trends from the previous study are, thus, consistent with the results from this examination [19].

Cracks in the concrete were observed even after the short exposure duration of only one month. The evolution of microcracks in ordinary Portland cement concrete due to the embedding of aluminum has been observed before through acoustic emission detection [26,27].

4.3. X-Ray Imaging

On the X-ray scans (Figure 6), the surfaces are sharply visible for the uncorroded sample, while the outer borders of the samples corroded for nine months seem to be less visible, which is consistent with the ongoing corrosion of the alloy and the formation of an oxidation layer [1,6–8]. This was also proven by the X-ray scan of the sample corroded in concrete after one year. The edges were not distinctly visible anymore and the sample surface was surrounded by a black layer, which could be considered to be hydrogen bubbles [1,4,6,9,10], and/or more likely, in concrete, the formed oxidation layer [1,6–8]. These observations support the observed data for the corrosion rates. They also point out the difficulty of imaging the R2 alloy in concrete due to the similar densities of aluminum and the oxide.

5. Conclusions and Future Outlook

The corrosion of the Studsvik R2 alloy under simulated repository conditions was examined by hydrogen gas-induced pressure build-up and mass loss evaluation. Both methods gave consistent trends that were in line with results from previous studies. This confirmed the trend of the R2 alloy corroding slower than pure aluminum metal in CW, as shown in Table 1. In concrete, the corrosion rate of the R2 alloy is similar to that of pure aluminum, although the aluminum corrosion rates show an increase after two years [1].

Table 1. Corrosion rates of R2 alloy in concrete compared to a previous study of aluminum metal under repository conditions [1].

	Corrosion Rate [µm/y]			
	1 Month	**6 Months**	**12 Months**	**24 Months**
R2 alloy in concrete	652 ± 44 *	161 ± 34 **	155 ± 26 **	-
R2 alloy in CW	257 ± 33 *	55 ± 8 **	3 ± 7 **	-
Al in concrete [1]	757 ± 333	164 ± 27	70 ± 11	114 ± 7
Al in CW [1]	1428 ± 178	214 ± 42	103 ± 17	54 ± 17

* Duplicate measurements in autoclaves, ** triplicate measurements of mass loss.

Nevertheless, the high initial corrosion rates due to hydrogen build-up could possibly lead to cracks in the concrete under repository conditions, which could be pathways for radionuclides. To prevent this, further studies will be conducted with different concrete compositions, such as the part replacement of CEM I by fly ash or magnesium phosphate or magnesium oxysulfate cement. Both are more climate-friendly with lower CO_2 production footprints and have the advantage of a lower pH, which could slow down the corrosion of aluminum. Further studies will also be conducted with other reactive metals that are relevant for Swedish repositories. Continuing deconstructive examinations will help analyze the oxide layer thickness by methods such as scanning electron microscopy. Ongoing exposures will determine if the long-term corrosion rates can be, as assumed by the linear dependency between corrosion in both media, evaluated in simplified cement–water solu-

tions instead of the more complex Portland cement concrete compositions. By acquiring more data, it is hoped that a better predictive model for corrosion rates can be tested.

Author Contributions: Conceptualization, M.S. and A.P.; methodology, M.S. and A.P.; software, M.S. and F.W.; validation, M.S. and A.P.; formal analysis, M.S.; investigation, M.S.; resources, M.S.; data curation, M.S.; writing—original draft preparation, M.S.; writing—review and editing, A.P., T.R.V., C.E., S.H.; visualization, M.S.; supervision, A.P.; project administration, A.P.; funding acquisition, A.P. and S.H. All authors have read and agreed to the published version of the manuscript.

Funding: This research received no external funding.

Data Availability Statement: The raw data supporting the conclusions of this article will be made available by the authors on request.

Acknowledgments: AB Svafo as well as the Swedish Nuclear Fuel and Waste Management Co. (SKB) are greatly acknowledged for funding this research. Chalmers Building Materials Lab is acknowledged for providing material for concrete.

Conflicts of Interest: Author Fredrik Wennerlund was employed by the company Tandläkare Fredrik Wennerlund; Author Svante Hedström was employed by the company SKB AB; Author Anders Puranen was employed by the company AB SVAFO. The remaining authors declare that the research was conducted in the absence of any commercial or financial relationships that could be construed as a potential conflict of interest.

References

1. Herting, G.; Odnevall, I. Corrosion of Aluminium and Zinc in Concrete at Simulated Conditions of the Repository of Low Active Waste in Sweden. *Corros. Mater. Degrad.* **2021**, *2*, 150–163. [CrossRef]
2. Santana, L.P. Management of radioactive waste: A review. *Proc. Int. Acad. Ecol. Environ. Sci.* **2016**, *6*, 38.
3. SSM (Swedish Radiation Safety Authority). Kingdom of Sweden—ARTEMIS. Self-Assessment Report 2023. In the IAEA Integrated Review Service for Radioactive Waste and Spent Fuel Management, Decommissioning and Remediation (ARTEMIS). 2023. Available online: www.ssm.se (accessed on 21 April 2025).
4. Kinoshita, H.; Swift, P.; Utton, C.; Carro-Mateo, B.; Marchand, G.; Collier, N.; Milestone, N. Corrosion of aluminium metal in OPC- and CAC-based cement matrices. *Cem. Concr. Res.* **2013**, *50*, 11–18. [CrossRef]
5. Atkins, M.; Glasser, F. Application of Portland cement-based materials to radioactive waste immobilization. *Waste Manag.* **1991**, *12*, 105–131. [CrossRef]
6. Tabrizi, M.; Lyon, S.; Thompson, G.; Ferguson, J. The long-term corrosion of aluminium in alkaline media. *Corros. Sci.* **1991**, *32*, 733–742. [CrossRef]
7. Ezuber, H.; El-Houd, A.; El-Shawesh, F. A study on the corrosion behavior of aluminum alloys in seawater. *Mater. Des.* **2008**, *29*, 801–805. [CrossRef]
8. Xiao, F.; Yang, R.; Liu, Z. Active aluminum composites and their hydrogen generation via hydrolysis reaction: A review. *Int. J. Hydrog. Energy* **2022**, *47*, 365–386. [CrossRef]
9. Pyun, S.-I.; Moon, S.-M. Corrosion mechanism of pure aluminium in aqueous alkaline solution. *J. Solid State Electrochem.* **2000**, *4*, 267–272. [CrossRef]
10. Jana, D.; Tepke, D.G. Corrosion of aluminum metal in concrete–A case study. In Proceedings of the 32nd International Conference on Cement Microscopy, ICMA, New Orleans, LA, USA, 28–31 March 2010; pp. 33–65.
11. Husaini, M.; Usman, B.; Ibrahim, M.B. Evaluation of corrosion behaviour of aluminum in different environment. *Bayero J. Pure Appl. Sci.* **2018**, *11*, 88–92. [CrossRef]
12. Mauret, P.; Lacaze, P. Water corrosion studies of AlMg (5154) and AlCuMg (2024) aluminium alloys by gas chromatography. *Corros. Sci.* **1982**, *22*, 321–329. [CrossRef]
13. Jones, R.H.; Vetrano, J.S.; Windisch, C.F. Stress Corrosion Cracking of Al-Mg and Mg-Al Alloys, December 2004. *Corrosion* **2004**, *60*, 1144–1154. [CrossRef]
14. Thomas, S.; Medhekar, N.V.; Frankel, G.S.; Birbilis, N. Corrosion mechanism and hydrogen evolution on Mg. *Curr. Opin. Solid State Mater. Sci.* **2015**, *19*, 85–94. [CrossRef]
15. King, A.D.; Birbilis, N.; Scully, J.R. Accurate electrochemical measurement of magnesium corrosion rates; a combined impedance, mass-loss and hydrogen collection study. *Electrochim. Acta* **2014**, *121*, 394–406. [CrossRef]

16. Curioni, M. The behaviour of magnesium during free corrosion and potentiodynamic polarization investigated by real-time hydrogen measurement and optical imaging. *Electrochim. Acta* **2014**, *120*, 284–292. [CrossRef]
17. Yang, Y.; Scenini, F.; Curioni, M. A study on magnesium corrosion by real-time imaging and electrochemical methods: Relationship between local processes and hydrogen evolution. *Electrochim. Acta* **2016**, *198*, 174–184. [CrossRef]
18. Song, G.; Atrens, A.; StJohn, D. An hydrogen evolution method for the estimation of the corrosion rate of magnesium alloys. In *Essential Readings in Magnesium Technology*; Springer International Publishing: Cham, Switzerland, 2016; pp. 565–572.
19. Schobel, M.; Ekberg, C.; Vollmer, T.R.; Puranen, A. Corrosion Characteristics of Studsvik R2 Al-Alloy by Hydrogen Evolution Under Simulated Repository Conditions. In Proceedings of the WM2025 Conference, Phoenix, AZ, USA, 9–13 March 2025.
20. Galvele, J.R. Transport processes and the mechanism of pitting of metals. *J. Electrochem. Soc.* **1976**, *123*, 464. [CrossRef]
21. Kanehira, S.; Kanamori, S.; Nagashima, K.; Saeki, T.; Visbal, H.; Fukui, T.; Hirao, K. Controllable hydrogen release via aluminum powder corrosion in calcium hydroxide solutions. *J. Asian Ceram. Soc.* **2013**, *1*, 296–303. [CrossRef]
22. Henry, P. Diffusion in absorbing media. *Proc. R. Soc. Lond. Ser. A Math. Phys. Sci.* **1939**, *171*, 215–241.
23. Van Gerven, T.; Cornelis, G.; Vandoren, E.; Vandecasteele, C. Effects of carbonation and leaching on porosity in cement-bound waste. *Waste Manag.* **2007**, *27*, 977–985. [CrossRef]
24. Berner, U. Evolution of pore water chemistry during degradation of cement in a radioactive waste repository environment. *Waste Manag.* **1992**, *12*, 201–219. [CrossRef]
25. Hoch, A.; Baston, G.; Glasser, F.; Hunter, F.; Smith, V. Modelling evolution in the near field of a cementitious repository. *Mineral. Mag.* **2012**, *76*, 3055–3069. [CrossRef]
26. Spasova, L.; Ojovan, M. Acoustic emission detection of microcrack formation and development in cementitious wasteforms with immobilised Al. *J. Hazard. Mater.* **2006**, *138*, 423–432. [CrossRef] [PubMed]
27. Spasova, L.; Ojovan, M. Characterisation of Al corrosion and its impact on the mechanical performance of composite cement wasteforms by the acoustic emission technique. *J. Nucl. Mater.* **2008**, *375*, 347–358. [CrossRef]